Eighth International Conference on
STEEL AND ALUMINIUM STRUCTURES
Edited by B. Young
Hong Kong, China, December 7 – 9, 2016

SHEAR BUCKLING OF LEAN DUPLEX STAINLESS STEEL PLATE GIRDERS WITH NON-RIGID END POSTS

Maarten FORTAN[a], Kristof DE WILDER[b], Dimitri DEBRUYNE[c] and Barbara ROSSI[b]

[a] Department of Civil Engineering, KU Leuven, Belgium
PhD Fellowship of the Research Foundation Flanders
Email: maarten.fortan@kuleuven.be

[b] Department of Civil Engineering, KU Leuven, Belgium
Emails: kristof.dewilder@kuleuven.be, barbara.rossi@kuleuven.be

[c] Department of Materials Engineering, KU Leuven, Belgium
Email: dimitri.debruyne@kuleuven.be

Keywords: Stainless steel structures; Shear buckling; Digital Image Correlation; Non-rigid end post.

Abstract. *This paper presents an experimental and numerical study of lean duplex stainless steel plate girders with non-rigid end posts. The test programme includes one I-section plate girder made of carbon steel and two tests on stainless steel girders, which will be achieved in the future. Advanced stereovision digital image correlation (DIC) was employed to continuously measure the deformed shape, and the corresponding three-dimensional displacements of the specimens, which enabled the full deformation history of the whole web of the plate girder to be traced. In parallel to the experimental investigation, a finite element study was also conducted. Preceded by validation of the FE models against the test results, parametric analyses were carried out to generate additional structural performance data for specimens made of lean duplex. The numerically derived data were carefully analysed and used to assess the accuracy of the current European design rules, in order to give directions for improvement. The comparisons showed that the European code leads to acceptable strength predictions, though further improvements remain possible.*

1 INTRODUCTION AND LITERATURE REVIEW

1.1 Duplex stainless steel grades

The duplex stainless steel family presents a microstructure made of austenite and ferrite. As a result these grades share the properties of both the austenitic and ferritic families, while being mechanically stronger than either family [1]. More specifically, the stainless steel grades EN1.4162 and EN1.4062 (also known as "lean" duplex), included in the latest revisions of Eurocode 3 Part 1-4 [2], are characterized by a low nickel content (ranging from 1.5% to ≥ 3% in standard duplex), resulting in significant reduction in cost compared to austenitic and duplex grade equivalents. These grades also contain a higher level of nitrogen, giving a substantial increase in strength as well as in pitting and crevice corrosion resistance, which is situated

between that of EN1.4301 and EN1.4404 austenitic grades. Moreover, they can be easily welded using the same processes as the ones used for the other stainless steel families.

Although stainless steel has been widely used in architecture, especially the austenitic family in facades and roofs thanks to its aesthetic expression, it was scarcely but increasingly used in structures, as load-carrying elements. Concerning bridges, stainless steel is usually chosen in recognition of its long-lasting appearance combined with low maintenance requirement in aggressive environments. Duplex grades have occasionally been used in bridges: the EN1.4462 grade in the Millennium footbridge in York (Whitby bird and partners), the lean duplex EN1.4162 grade in the Siena bridge in Ruffolo (Eng. Pistoletti), in the Sölvesborg bridge in Sweden (Ljusarkitektur) and in the Sant Fruitós footbridge in Barcelona (Pedelta Structural Engineers), or the EN1.4362 grade in the Arco Ponte Malizia arch bridge in Siena (Eng. Pistoletti), [3] to [10]. The structural element shapes often include long horizontal elements with large plates susceptible to shear buckling (Figure 1).

Figure 1. Example of a bridge made of duplex EN1.4162 grade: Siena footbridge.

1.2 Shear buckling

The present paper deals with the shear buckling of flat rectangular plates encountered in prismatic welded members, such as I-profile beams. Submitted to monotonically increasing in-plane loading (I-profile beam in bending), relatively slender webs may fail by shear buckling i.e. out-of-plane deformation occurring at 45° in the web-panel subjected to shear. In the present experimental and numerical analyses, welded girders failing by a shear dominant failure mode involving shear buckling are studied. The experiment presented herein is conducted on a specimen made of carbon steel and used to validate a first finite element model (FEM). According to literature, the experimental study of lean duplex girders with non-rigid end post has not yet been achieved. So far, EN1.4162 plate girders with rigid end post [11] and EN1.4462 plate girders with non-rigid end post [12] were investigated. Our first FEM was hence further modified and used to model these reference experiments made on stainless steel girders. Subsequently, a parametric analysis investigating lean duplex welded girders with non-rigid end post was carried out. The outcomes of this analysis are presented in this paper.

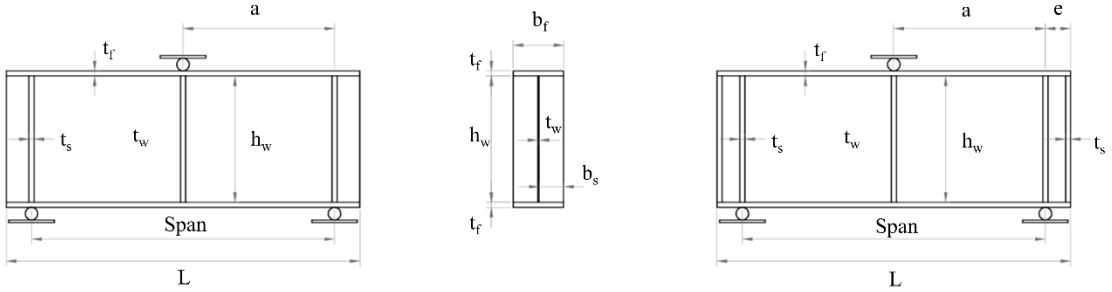

Figure 2. Plate girder. Left: non-rigid end post, right: rigid end post.

1.3 Literature review

Shear buckling of carbon steel plate girders has been extensively studied in the past because of the high resistance-to-weight ratio of plate girders characterised by slender webs. In the last century, numerous theories have been developed to accurately describe the buckling and post-buckling behaviour of slender plate girders and predict their ultimate load. The fact that so many researchers devoted their time to this subject confirms its importance and complexity. Shear buckling was extensively studied in [13] and [14], where an approximate solution for the buckling coefficient k_τ was derived. One of the first to have broadly tested and described the behaviour of steel panels failing by shear buckling was Basler [15]. According to Basler, the shear resistance can be obtained by combining the post buckling resistance through the development of a tension field in the web and the critical elastic buckling load, without taking into account any contribution of the flanges. Later, Porter in [16] integrated the contribution of the flanges to the post buckling strength. This method is at the root of both the American and European design rules. However, the tension field concept is only applicable to aspect ratios smaller than 3 but is unusable to predict the shear buckling resistance of beams with wider aspect ratios. To describe the resistance of both stiffened and unstiffened webs, Höglund [17] developed the rotated stress field theory based on a database of over 350 experiments on the shear buckling behaviour of steel and aluminium beams. This method takes into account the contribution of the web, flanges and longitudinal or transverse stiffeners and forms the basis of the current EN 1993-1-5 [18] design rules. Shear buckling in stainless steel beams was first investigated by Carvalho [19] and, in 2001, Olsson [12] adapted the design rules, which were implemented in EN 1993-1-4 [2]. These design rules included the web and flange contributions without taking into account end post rigidity. A great amount of research is still ongoing on this subject such as, for instance, on composite girders with concrete slabs, [20] and [21], in case of elevated temperatures or fire, [22] and [23], on high strength steel [24] and on stainless steel girders.

Austenitic stainless steels have been broadly studied in recent years, [25] to [29], and recent European projects have highlighted some of the main features of ferritics, [30], [31]. However, much less information is available regarding the duplex and lean duplex grades. For what concerns duplex grades, research mainly regarded the material properties in [32] and [33], the behaviour of stub and slender columns in [27] and [34] and the beam-columns behaviour in [35]. Welded I-sections columns were studied in [36] and lean duplex beams in [37][38]. Research concerning the welding of lean duplex (EN 1.4162) was done by Westin in [39] and Sorrentino et al. in [40]. Residual stresses from welding stainless steel plates was investigated by Yuan et al. in [41] and by Gardner and Cruise in [42]. But, overall, there exists today a lack of experimental data on the stability of lean duplex fabricated beams, on their lateral-torsional buckling and shear buckling resistances. Specifically about shear buckling, a collection of the experiments conducted throughout the last decade is provided by Saliba et al. in [43], with 17 austenitic and 4 duplex shear buckling tests with non-rigid end post, [12], [44] and [45], and 4 austenitic and 9 lean duplex specimens with rigid end post, [11] and [45]. Moreover, numerical studies have been performed by Hassanein [46] and Estrada [47] leading to an improvement of the design rules for stainless steel plate girders. However, in these studies, no experimental data on lean duplex plate girders with non-rigid end posts are reported.

1.4 Stereovision digital image correlation

In this research the potential of digital image correlation (DIC) is explored to determine the full-field deformation history of the girder and its web during loading. DIC is an optical-numerical measuring technique that offers unique opportunities to determine the complex full-

field displacement and strain distribution at the surface of objects under arbitrary loading in 2D and 3D, depending on the number of cameras used – a single camera in the case of 2D, two or more cameras in the case of 3D. In 1983, Sutton et al. [48] developed and tested 2D-DIC, upon which numerous research domains started applying this method. In 1993, stereovision DIC was pioneered by Chao et al. [49]. Unlike 2D-DIC, a stereovision camera system is not limited to in-plane displacements, but allows for the displacement and strain evaluation at the surface of 3D shapes.

The basic principle is as follows. Charged-Coupled Device (CCD) cameras take synchronized images of a specimen or object in the undeformed and deformed state, a stage which is referred to as the optical part of DIC. Those cameras use a small, rectangular piece of silicon, which has been partitioned into an array of light-sensitive cells. Each cell represents one pixel of the image that is generated. Through digitization, the charge of each light-sensitive cell is transformed into a certain grey scale value (ranging from 0 to 255 in the case of 8-bit images). Therefore an image can be looked at as a 2 dimensional discrete function $g(x, y) \in R$ in which each element represents the grey value of the corresponding pixel. Afterwards, these images are computationally compared (correlated) in a correlation software, representing the numerical part of DIC. First, a certain pixel and its neighbourhood is selected in the undeformed image. The combination of such a pixel and its neighbourhood is called a subset. Next, the correlation algorithm traces this same subset in the deformed image by minimization of a cost function (the so-called cross-correlation coefficient). During this correlation procedure the subset can change size and shape to take into account the deformation of the specimen. The result of this optimization procedure is the displacement of the centre pixel of the subset. In this way the entire image is scanned; each time the subset is moved a certain number of pixels (px) in the x- or y-direction, defined by the step size, to determine the displacement. Finally one obtains the complete displacement field at the surface of the specimen under consideration, and, by derivation, also the strain field.

It should be noted that the correlation procedure is only feasible if the surface of the specimen is covered with a random pattern. In general, one applies paint onto the specimen's surface with an aerosol to obtain a random speckle pattern. This random pattern generates a unique signature for each subset so that it can be retrieved from the deformed image. Figure 3 shows an example of such a random speckle pattern and shows how the subset (red square) from the undeformed image is transformed in the deformed image.

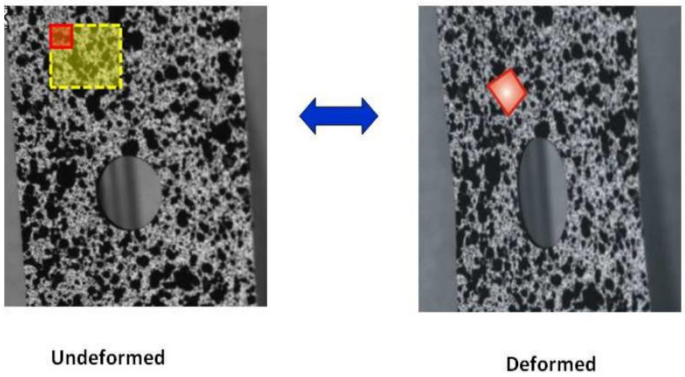

Figure 3: Correlation of a subset between the undeformed (left) and deformed image (right).

As the DIC method relies on digital images to measure deformation, the quality of the images determines the quality of the measurements. The image quality depends on the experimental

setup and on adequate preparations in order to minimise errors. It is hard to unambiguously define the accuracy of the DIC technique however it is generally accepted that an accuracy between 2% and 5% of the pixel size can be achieved in decent experimental conditions. All of these error sources are discussed in detail in [50], the most important being:

- Noise (on the grey scale values), which occurs due to the quantization of the grey scale values when converting the analogue signal to a digital signal. This noise, introducing non-existing gray level fluctuations, results in artificial displacements when the difference between the reference and the deformed image is minimised. The effect of noise can be reduced considerably by using high performance hardware in combination with filtering and/or averaging of images.
- Light conditions: perfect homogeneous light conditions are hard to obtain. In most applications, a change in light intensity is present across the image. Also during the capturing of the deformed images, a change in illumination can occur. This change of light affects the correlation procedure, but can be largely resolved by using appropriate correlation criteria.
- Image distortion due to the use of wide-angle lenses or zoom lenses. Several methods exist to compensate for this lens distortion.
- The subset shape order and the subset size: the subset should be large enough to contain sufficient features while - at the same time - small enough to represent the underlying deformation. Increasing the shape function of the subset in order to enhance the capability of representing the deformation is also an option, but increases the sensitivity to noise.
- The sub-pixel interpolation filter: to obtain a sub-pixel displacement accuracy in DIC, the gray levels and their gradients have to be interpolated from the regular grid structure which causes a positional error
- The speckle pattern: a pattern can vary in characteristics such as contrast, gradients or speckle size. Many guidelines exist to assess the quality of the speckle pattern.

As far as the authors know, this is the first shear buckling test measured with DIC and one of the first capacity or stability tests of steel beams to which this method is applied. Nonetheless, both 2D- and 3D-DIC have been used in a variety of civil engineering applications. For example, Küntz et al. [51] employed DIC to gather information on the development of cracks in a reinforced concrete beam of the Saint-Marcel bridge during a static loading test. Yoneyama et al. [52] and Malesa et al. [53] measured deflections of steel bridge girders whilst a heavy cargo truck or a train was passing on. Malesa et al. [53] also measured the displacements of a girder close to a connection. DIC was applied by Koltsida et al. [54] and Santini-Bell et al. [55] for monitoring, respectively, a masonry arch bridge and a steel girder composite bridge.
Besides structural health monitoring or inspection, this method was implemented for measurements during in situ and laboratory tests. Tung et al. [56] used DIC to measure deformations during an in situ pushover test of an old building columns retrofitted with steel plate. In laboratory, DIC has been used to study various materials, e.g. canvas paintings [57], composites [58][59], aluminium [60] and the most common construction materials: concrete and steel. Ferreira et al. [61], Dutton et al. [62] and Souid et al. [63], Smith et al. [64] and De Wilder [65] applied stereovision DIC to obtain the displacement field in concrete beams. Ghafoori and Motavalli [66] investigated the fatigue and fracture behaviour of a steel I-beam. They employed DIC to illustrate the stress evolution pattern and the plasticity zone around the crack tip. Hild et al. [67] applied DIC to identify the behaviour of steel beams prior to and after the initiation of local buckling. Kujawinska et al. [57] tested a metal-plate arch and monitored displacement maps with DIC. Sozen and Guler [68] investigated a bolted steel connection and

compared in-plane displacement distributions computed through DIC and strain gauges. Shih and Sung [69] tested a five-story shearing steel structure under dynamic loading and measured the responses by means of a single camera with 3D images. This is achieved by separating the view axis of the camera with a spine-type prism, which allows to store two images in one photo. Tran et al. [70] executed a compression test on a down scale model of a steel tubular wind turbine tower to study buckling around the door opening of the tower using DIC. An extensive list of applications of both 2D- and stereovision DIC in various research domains can be found in Orteu [71] and Sutton [50].

2 EXPERIMENTAL STRUCTURAL PERFORMANCE OF A CARBON STEEL PLATE GIRDER

2.1 Testing set-up

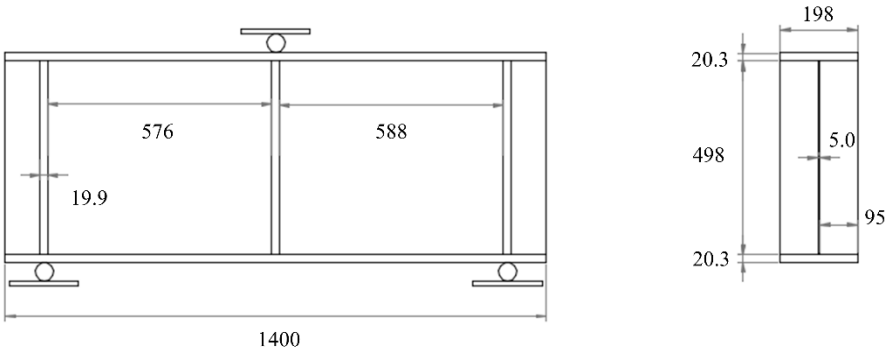

Figure 4: Dimensions of the tested carbon steel beam

An experimental programme, comprising material tensile tests, measurements of geometric imperfections and one test on a carbon steel plate girder, is described in this section. The complete test programme also includes two I-section plate girders made of duplex stainless steel, which will be performed in the future. All the tests are carried out in the Materials & Structures Laboratory of the Department of Civil Engineering at KU Leuven, TC De Nayer. The carbon steel specimen, Figure 4, was welded using Submerged Arc Welding (SAW), an automatic method with high productivity which is used for thick sections (>10 mm) and for large specimens. Whereas, to weld the duplex stainless steel specimens, Gas Metal Arc Welding (GMAW) will be used. A three point bending test was performed on a specimen with dimensions provided in Figure 4. The section had Class 4 webs in bending according to EN 1993-1-4 [2] and non-rigid end post conditions were achieved at each support. A total of 5 digital displacement transducers combined with stereovision DIC were used to monitor the development of the shear buckling during the tests and to validate the numerical models.

Two AVT cameras with a resolution of 5Mpixel combined with 12mm lenses, were used as the stereovision DIC set-up, and were placed at approximately 2m of the specimen to get a full view of the specimen. The speckle pattern, with a speckle size ranging from 2.5 to 5mm (5 to 10 px), was applied by transferring a laser printed pattern from paper to a white primer coating, painted onto the steel surface, using a solvent. Synchronized images were taken at a frequency of 1Hz and processed afterwards using MatchID [72]. The processing step used the zero-normalized sum of squared difference correlation algorithm to determine the displacements of each subset with a size of 31px and a step of 5px in combination with bicubic spline interpolation and an affine shape function.

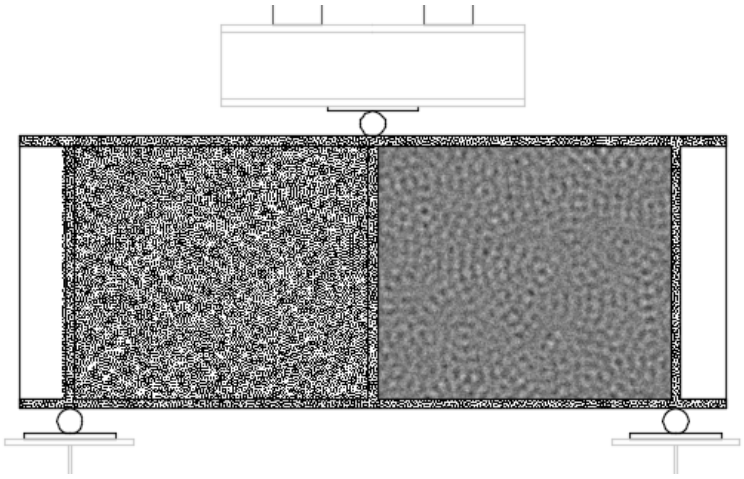

Figure 5: Test set-up and speckle pattern

2.2 Material mechanical behaviour

Characterisation of the material behaviour was achieved via 8 tensile dog-bone coupon tests (4 in the longitudinal direction i.e. parallel to the rolling direction and 4 in the transverse direction, according to EN 6892 [73]), during which the strain field was measured using both DIC and a traditional digital extensometer. The DIC video extensometer uses two selected subsets as can be seen from Figure 6. The whole coupon was speckled with speckles small enough to allow a good correlation between both measurements up to necking of the specimen, as illustrated in Figure 7. The strain rate used for all of the material tests was 0.007 % / s before yielding and 0.025 % / s after.

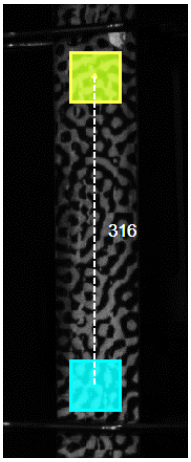

Figure 6: DIC video extensometer

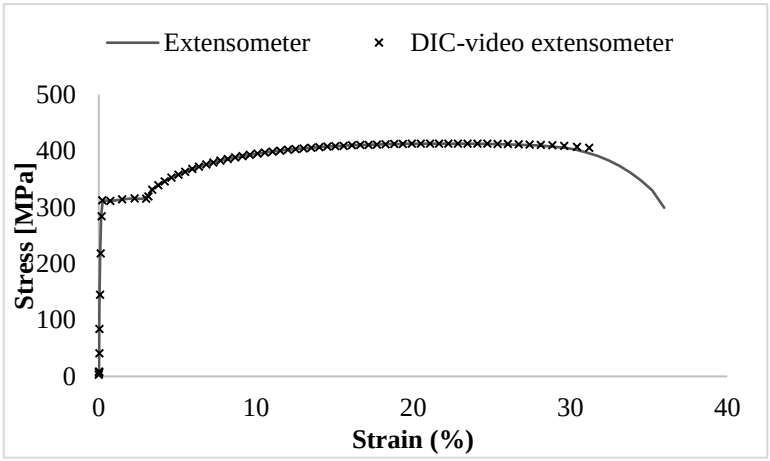

Figure 7: Measured stress-strain curve for carbon steel with extensometer and stereovision DIC

The yield strength in the transverse direction, on average 311 MPa, is 7% higher than in the longitudinal direction, on average 290 MPa. However, the length of the yield plateau, the ultimate strength σ_u, on average 413 MPa, and ultimate strain ε_u, on average 22 %, are similar for all tests.

2.3 Initial imperfection

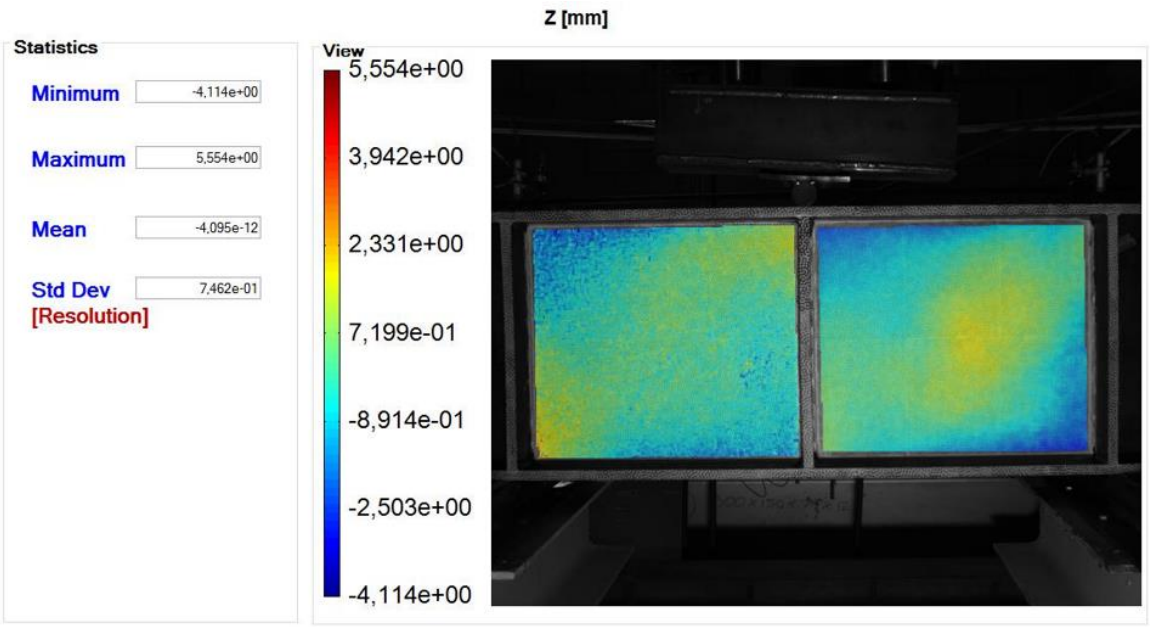

Figure 8: Local geometrical imperfection in the web-panels according to DIC measurements

Prior to testing, the initial geometry of the plate girders was assessed using DIC. According to the measurements, the local geometrical imperfection in the tested carbon steel girder is a combination of a plate undulation at 45° in the web and a slight bow in the flanges. The maximum relative amplitude of the waves in the web equals 2.5mm mm corresponding to $h_w/200$. Following the welding procedure, the imperfection shape tends to occur in the same direction than the shear buckling wave in the right web-panel, and, noticeably, in the opposite direction in the left panel (Figure 8). The measured imperfections fall in the range of the geometric fabrication tolerances for welded components (class 1) provided in EN 1090-2 [74], i.e. web curvature $\Delta = \pm h_w/100 \geq 5mm$

2.4 Test result

The girder fails by shear involving shear buckling of the plate girder web. The key experimental results from the plate girder test are $V_{u,test}$ =412kN and $M_{u,test}$ = 241kN.m, respectively, the applied shear force and bending moment at failure. The following two images (Figure 9) present the raw out-of-plane displacement field in mm measured using DIC. Each picture corresponds to a particular load step as highlighted. In the following section, the results of this experiment together with the results of Saliba [11] are employed for the validation of the FE models.

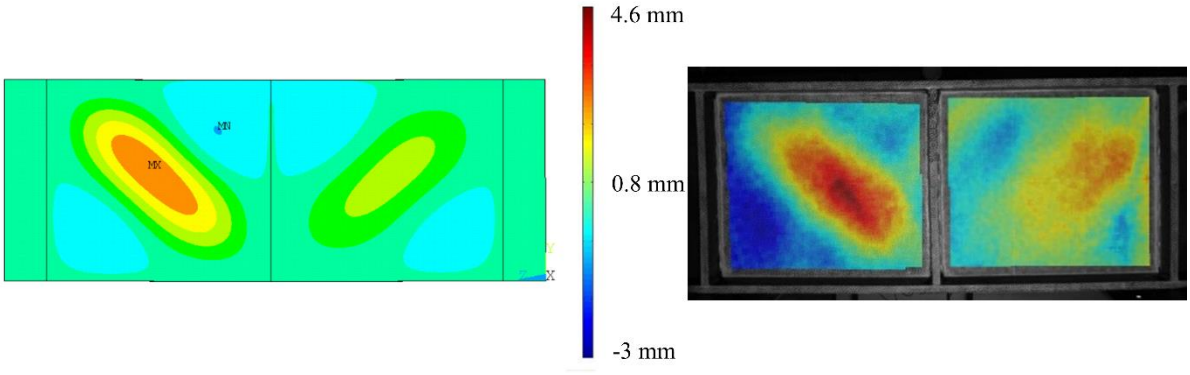

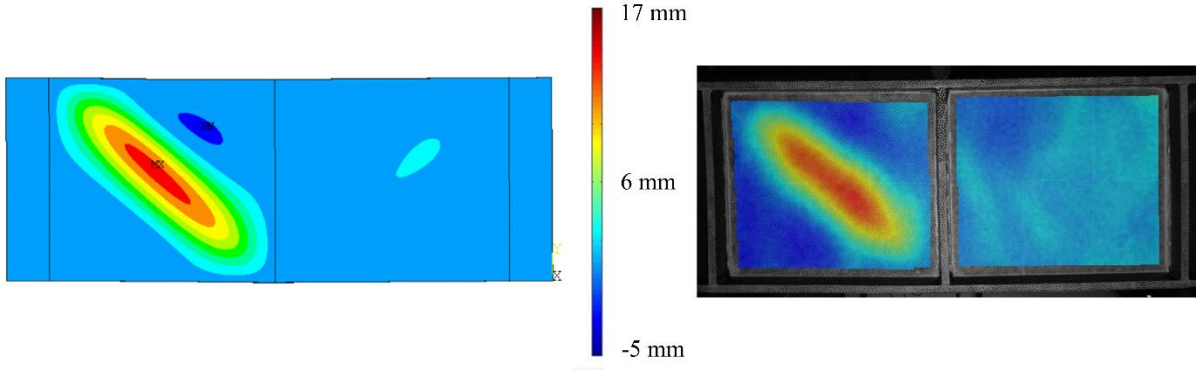

Figure 9:Out of-plane displacement field in the web-panel for (up) N=815kN (buckling) and (down) N=738kN (post buckling) – left: FEM, right: DIC raw measurements.

3 NUMERICAL STRUCTURAL PERFORMANCE OF LEAN DUPLEX STAINLESS STEEL PLATE GIRDERS

3.1 FEM validation

A geometrically and materially nonlinear analysis using the FE method has been conducted to evaluate the resistance of welded girders suffering shear buckling. In the present work, the nonlinear FEM package ANSYS was used.

Shell elements were employed to discretize the model. The SHELL181 element, a general purpose shell element with four nodes and reduced integration to form the element stiffness, was used to simulate the web, flanges and stiffeners (quadratic shell finite elements SHELL281 were shown to bring no additional information). The measured geometrical dimensions were used in the FE models intended for calibration against the tests (both the test presented above and the tests of Saliba [11]). Since a common node was used for the web and flange modelling, there exists an overlapping area of $t_f/2 \times t_w$ mm^2. Also, the area of the weld is neglected. Both hypotheses were shown to have no influence on the numerical results.

One way to simulate the boundary condition is to fix the bottom part of the specimen along the flanges (simply supported boundary conditions), while the top is allowed to move freely. The displacement is imposed on three nodes along the top flange, in the middle of the beam.

The adopted material model is, for both comparisons, the measured average (between the longitudinal and transverse directions) material model presented above for carbon steel, Figure 7, and from Saliba [11] for the duplex stainless steel grade EN 1.4162.

The model includes an initial geometrical imperfection that corresponds to the lowest buckling mode shape scaled using the measured amplitude. Another aspect in the modelling of the H-shaped profiles concerns the development of local plate buckling. The zone at the intersection of the flanges or stiffeners and the web remains unaffected by the extent of local buckling. It is possible to model this through a truss system added in the web-flange junction zone meant to keep this zone rigid. Nevertheless, it was shown to have very little influence on the numerical results.

The influence of the longitudinal residual stresses were assessed for both the carbon steel cross-section [75] and the stainless steel case cross-section.

A good correlation between the FEM and the DIC measurements for the shape and magnitude of the out of plane displacements of the web in the buckling and post-buckling domain was achieved (Figure 8). The following figure illustrates the accuracy of the FEM against the experimental results for stainless steel girders.

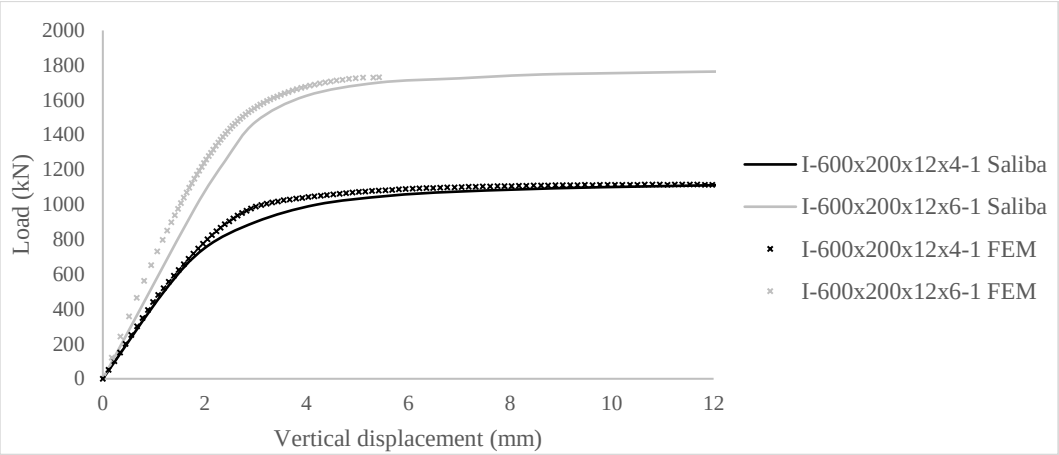

Figure 10: Load versus mid-span vertical displacement for two tests from Saliba [11]

3.2 Numerical results for the lean duplex stainless steel grade EN 1.4062

The suitability of the numerical models for performing parametric studies was assessed in the previous paragraphs by comparing the experimental results to the FE simulations. Using the validated FEM, a series of parametric studies were achieved to calculate the resistance of lean duplex welded girders with non-rigid end posts, over a certain range of aspect ratios. The study covers 6 web thicknesses to cover a range of web slenderness from 0.74 to 3.40. All the sections are Class 4. For h_w = 500mm, the aspect ratio a/h_w is varied between 0.8 to 4. But for the other studied web heights (400, 600 and 750), the aspect ratio is kept to 1.0. The flange thickness is kept unchanged and non-rigid end posts are employed. The material characteristics used in the FE parametric studies are based on measurement on dog-bone tensile coupon tests (Figure 11), for which E = 199700N/mm², $\sigma_{0.2}$ = 541N/mm², $\sigma_{1.0}$ = 607N/mm², σ_u = 726N/mm, n = 11.6 and m = 3.1 [1]. The imperfection corresponds to the lowest buckling mode shape scaled by the recommended equivalent amplitude in EN 1993-1-5 [18].

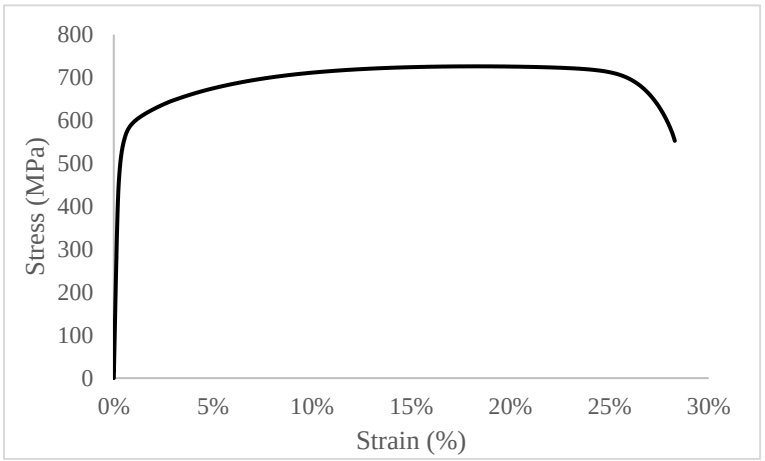

Figure 11: Measured stress-strain curve for lean duplex stainless steel EN1.4062

All failure modes are shear dominant failure modes as $V_{u,FEM}/M_{u,FEM} > V_{bw,Rd}/M_{f,Rd}$. Typical FE failure modes for the lean duplex plate girders are shown in Figure 12 and Figure 13 for two different aspect ratios.

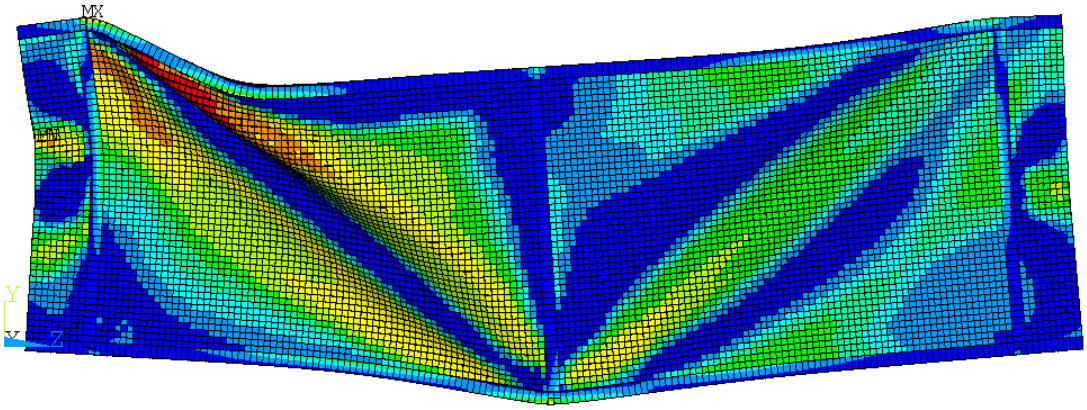

Figure 12: Typical failure mode for a 500x200x20x4 girder with an aspect ratio of 1.5

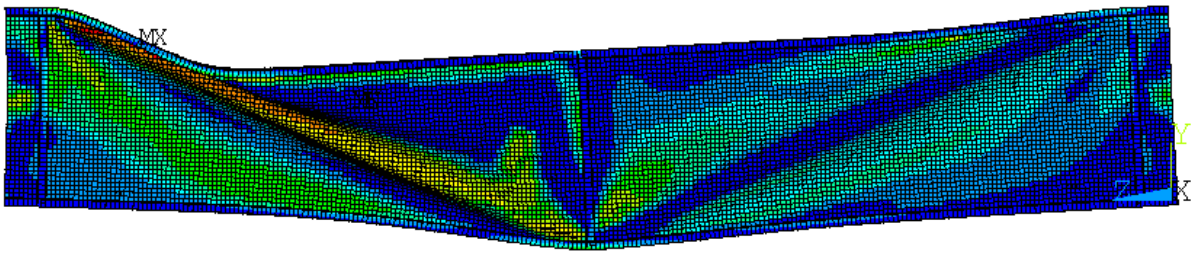

Figure 13: Typical failure mode for a 500x200x20x3 girder with an aspect ratio of 4

4. COMPARISON WITH EN 1993-1-4 (2006)

These numerical results are then used to assess the suitability of the current codified design provisions to lean duplex stainless steel plate girders, with non-rigid end post.

4.1 Design rules

The shear buckling design rules for steel structures can be found in EN 1993-1-5 [18] with additional rules for stainless steel in EN 1993-1-4 [2]. Despite the material characteristics shown by the stainless steel grades, the design concept, based on the rotated stress field theory, is however the same in both documents. When the requirement for the web slenderness h_w/t is not satisfied (equations 1 and 2), the resistance needs to be checked.

Stainless steel unstiffened web: $$\frac{h_w}{t} < \frac{56.2}{\eta}\varepsilon \quad (1)$$

Stainless steel stiffened web: $$\frac{h_w}{t} < \frac{24.3}{\eta}\varepsilon\sqrt{k_\tau} \quad (2)$$

For stainless steel, ε is provided by equation 3 and the shear buckling coefficient k_τ by equations 4 and 5. The value η = 1.20 is recommended for all stainless steel grades.

$$\varepsilon = \sqrt{\frac{235}{f_y}\frac{E}{210000}} \quad (3)$$

For $a/h_w \geq 1$ $$k_\tau = 5{,}34 + 4{,}00(h_w/a)^2 \quad (4)$$

For $a/h_w < 1$: $$k_\tau = 4{,}00 + 5{,}34(h_w/a)^2 \quad (5)$$

The web and flange contributions to the shear buckling resistance $V_{b,Rd}$ are calculated using equations 6 to 12, where λ_w is the web slenderness and χ_w is the reduction factor, which can be found in Table 1 for stainless steel.

$$V_{b,Rd} = V_{bw,Rd} + V_{bf,Rd} \leq \frac{\eta f_{yw} h_w t}{\sqrt{3}\gamma_{M1}} \quad (6)$$

$$V_{bw,Rd} = \frac{\chi_w f_{yw} h_w t}{\sqrt{3}\gamma_{M1}} \quad (7)$$

Transverse stiffeners at supports only:

$$\overline{\lambda}_w = \frac{h_w/t_w}{86.4\varepsilon} \quad (8)$$

Transverse stiffeners at supports and intermediate transverse or longitudinal stiffeners:

$$\overline{\lambda}_w = \frac{h_w/t_w}{37{,}4\varepsilon\sqrt{k_\tau}} \quad (9)$$

Table 1: Reduction factor χ_w for stainless steel beams

	Rigid end supports	**Non-rigid end supports**
$\boldsymbol{\overline{\lambda}_w < 0{,}65/\eta}$	η	η
$\boldsymbol{0{,}65/\eta \leq \overline{\lambda}_w} < 0.65$	$0{,}65/\overline{\lambda}_w$	$0{,}65/\overline{\lambda}_w$
$\boldsymbol{\overline{\lambda}_w \geq 0.65}$	$1{,}56/(0{,}91 + \overline{\lambda}_w)$	$1{,}19/(0{,}54 + \overline{\lambda}_w)$

When M_{Ed} is smaller than $M_{f,Rd}$ (the bending resistance considering the flanges only), a contribution to the shear buckling resistance can be added, see equation 10. The cooperating width and cooperating length c are calculated using respectively equation 11 and equation 12.

$$V_{bf,Rd} = \frac{b_f t_f^2 f_{yf}}{c\gamma_{M1}}\left[1 - \left(\frac{M_{Ed}}{M_{f,Rd}}\right)^2\right] \quad (10)$$

$$b_f = min(b_f; 15\varepsilon t_f) \quad (11)$$

$$c = a\left(0{,}17 + \frac{3.5 b_f t_f^2 f_{yf}}{t_w h_w^2 f_{yw}}\right) \quad (12)$$

4.2 Comparisons

The numerical to predicted ultimate shear forces ratio, $V_{Ed}/V_{b,Rd}$, is presented in Table 2, and is characterized by a mean value of 1.13 and a coefficient of variation (COV) of 0.09. It can be concluded that the current design rules give satisfying reliability.

In Figure 14, the ratios $V_{Ed}/V_{b,Rd}$ for all the numerical results are plotted versus the web slenderness λ_w. For specimens with a high flange contribution (unbalanced cross-sections), the numerical results diverge from the codified results. As it will be highlighted below, this is mainly due to the flange contribution present in EN 1993-1-4 which is unable to tackle their real behaviour.

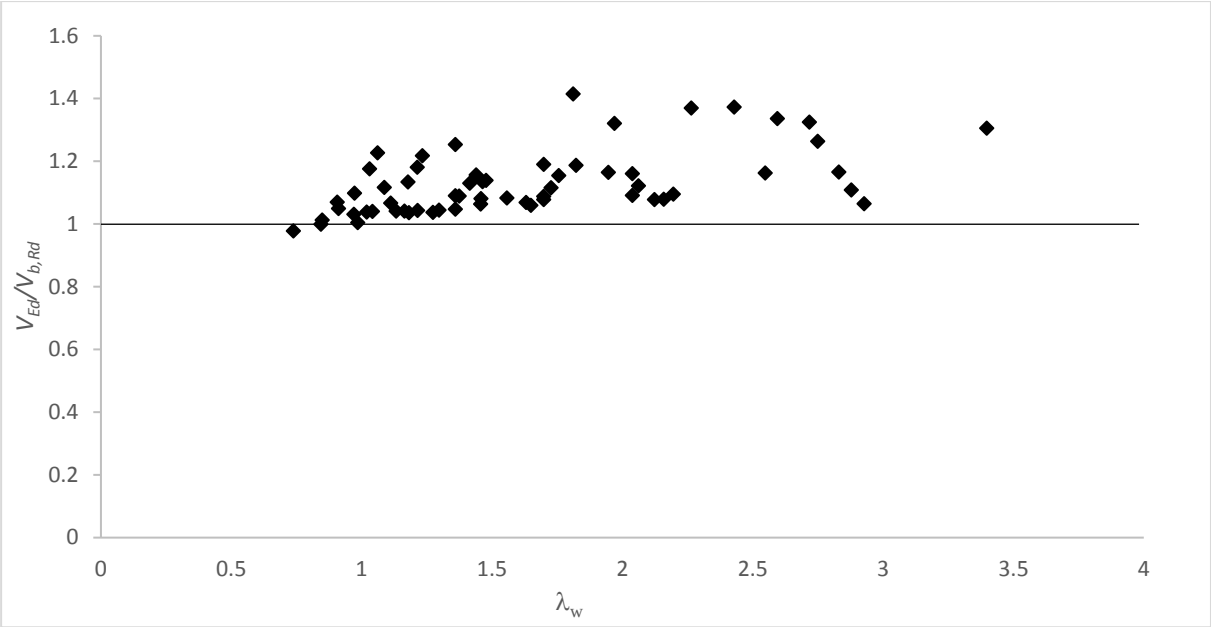

Figure 14: Utilisation ratio VEd/Vb,Rdr for the design rules provided in EN 1993-1-4

Table 2: Numerical and codified results (and utilization ratios) for the studied specimens

Name	$V_{u,FEM}$	$V_{b,Rd}$	$V_{u,FEM}/V_{b,Rd}$	$V_{b,Rd,\ imp.}$	$V_{Ed}/V_{b,Rd,\ imp.}$
-	kN	kN	-	kN	-
I400x200x20x3_a400	497	351	1.41	393	1.26
I400x200x20x4_a400	605	482	1.25	542	1.12
I400x200x20x5_a400	722	647	1.12	698	1.03
I400x200x20x6_a400	876	819	1.07	861	1.02
I500x200x20x3_a500	484	353	1.37	399	1.21
I500x200x20x4_a500	611	513	1.19	548	1.11
I500x200x20x5_a500	749	687	1.09	711	1.05
I500x200x20x6_a500	907	871	1.04	884	1.03
I500x200x20x7_a500	1095	1063	1.03	1067	1.03
I500x200x20x8_a500	1276	1259	1.01	1257	1.01
I600x200x20x3_a600	488	368	1.32	395	1.23
I600x200x20x4_a600	617	532	1.16	546	1.13
I600x200x20x5_a600	761	711	1.07	714	1.06
I600x200x20x6_a600	947	904	1.05	898	1.05
I600x200x20x7_a600	1153	1107	1.04	1095	1.05
I600x200x20x8_a600	1368	1318	1.04	1301	1.05
I750x200x20x3_a750	494	378	1.31	384	1.29
I750x200x20x4_a750	633	544	1.16	537	1.18
I750x200x20x5_a750	797	730	1.09	713	1.12
I750x200x20x6_a750	1006	933	1.08	910	1.10
I750x200x20x7_a750	1224	1150	1.06	1125	1.09
I750x200x20x8_a750	1431	1379	1.04	1354	1.06
I500x200x20x3_a400	550	416	1.32	473	1.16
I500x200x20x4_a400	680	597	1.14	641	1.06
I500x200x20x5_a400	820	791	1.04	821	1.00
I500x200x20x6_a400	999	995	1.00	1011	0.99

I500x200x20x7_a400	1204	1205	1.00	1211	0.99
I500x200x20x8_a400	1388	1420	0.98	1416	0.98
I500x200x20x3_a600	434	316	1.37	354	1.23
I500x200x20x4_a600	551	464	1.19	493	1.12
I500x200x20x5_a600	678	627	1.08	646	1.05
I500x200x20x6_a600	834	799	1.04	810	1.03
I500x200x20x7_a600	1019	980	1.04	983	1.04
I500x200x20x8_a600	1223	1165	1.05	1163	1.05
I500x200x20x3_a750	374	280	1.34	310	1.21
I500x200x20x4_a750	485	417	1.16	439	1.10
I500x200x20x5_a750	615	568	1.08	582	1.06
I500x200x20x6_a750	762	729	1.04	737	1.03
I500x200x20x7_a750	958	898	1.07	900	1.06
I500x200x20x8_a750	1177	1072	1.10	1070	1.10
I500x200x20x3_a1000	310	245	1.26	267	1.16
I500x200x20x4_a1000	416	371	1.12	387	1.07
I500x200x20x5_a1000	541	511	1.06	521	1.04
I500x200x20x6_a1000	720	661	1.09	666	1.08
I500x200x20x7_a1000	927	817	1.13	819	1.13
I500x200x20x8_a1000	1151	978	1.18	978	1.18
I500x200x20x3_a1250	262	225	1.17	242	1.08
I500x200x20x4_a1250	371	344	1.08	357	1.04
I500x200x20x5_a1250	520	477	1.09	485	1.07
I500x200x20x6_a1250	701	620	1.13	623	1.12
I500x200x20x7_a1250	908	769	1.18	769	1.18
I500x200x20x8_a1250	1130	921	1.23	921	1.23
I500x200x20x3_a1500	235	212	1.11	226	1.04
I500x200x20x4_a1500	353	327	1.08	337	1.05
I500x200x20x5_a1500	508	455	1.12	461	1.10
I500x200x20x6_a1500	686	593	1.16	595	1.15
I500x200x20x7_a1500	895	735	1.22	735	1.22
I500x200x20x3_a2000	208	195	1.06	206	1.01
I500x200x20x4_a2000	334	305	1.09	312	1.07
I500x200x20x5_a2000	493	427	1.15	430	1.15
I500x200x20x6_a2000	632	557	1.13	557	1.13
		AVG	1.13	AVG	1.10
		COV	0.09	COV	0.07

The flange contribution for carbon steel members is calculated using equation 13. When this equation is used to assess the flange contribution, some improvement can be achieved and the average of the utilization ratio decreases to 1.10 with a COV of 0.07.

$$c = a\left(0{,}25 + \frac{1.6 b_f t_f^2 f_{yf}}{t_w h_w^2 f_{yw}}\right) \tag{13}$$

5 CONCLUSION

In the present paper, shear buckling of stainless steel welded girders with non-rigid en post are investigated. First, a test achieved on one full-scale carbon steel welded I-profile is used to validate a finite element model (FEM). During this test, stereovision digital image correlation is used as the main measurement technique, to record the full field of displacements occurring in the web panels of the girder. These measurements were compared to the 3D displacement field obtained numerically and very good agreement of both the shape and amplitude of the bulge occurring at 45° further to shear buckling was obtained. The FEM predicted the experimental ultimate load with a relative difference of 2.3%. The second FEM reproduces the experiments performed by Saliba et al. in [11] on stainless steel girders and is able to accurately capture the experimental load versus vertical displacement for girders with non-rigid end post. Based on this preliminary validation of the FEM, a parametric study was carried out. The web thickness and height as well as aspect ratio a/h_w was varied to cover a range of web slenderness from 0.74 to 3.40. The ultimate loads were then predicted using the current design rules of EN 1993-1-4. The comparison of the numerically predicted ultimate loads with the theoretical ones led to an average utilization ratio of $V_{u,FEM}/V_{b,Rd}$ of 1.13 combined with a coefficient of variation (COV) of 0.09. However, it was shown that the flange contribution for stainless steel is not well predicted, especially when the flanges are not fully utilized to resist the bending moment, ($M_{Ed} < M_{f,Rd}$). Through the use of the cooperation length equation of EN 1993-1-5 for carbon steel, the theoretical predictions can be further improved and the average is reduced to 1.09, with a COV of 0.07. Further research will be achieved to improve or amend these conclusions.

6 ACKNOWLEDGEMENT

The first author is supported by the Research Foundation Flanders.

REFERENCES

[1] Arrayago I., Real E. and Gardner L., “Description of stress–strain curves for stainless steel alloys”, *Materials and Design*, Volume 87, pages 540-552, 2015.

[2] European Committee for Standardization (CEN), “Eurocode 3: design of steel structures - part 1-4: General rules - Supplementary rules for stainless steels.” Brussel Cen, 1/5/2005, Brussel, 2005.

[3] *Applications for Stainless Steel Long Products - A guide to unlocking all the properties of stainless*, International Stainless Steel Forum (ISSF), 2009.

[4] Gedge G., “Structural uses of stainless steel –buildings and civil engineering”, *Journal of Constructional Steel Research*, Volume 64(11),pages 1194-1198, 2008.

[5] Baddoo N. R., “Stainless steel in construction: A review of research, applications, challenges and opportunities”, *Journal of Constructional Steel Research*, Volume 64(11), pages 1199-1206, 2008.

[6] Esko M., “Stainless steel in architecture”, *Building Series*, Volume 9, Euro Inox, 2005.

[7] International Iron & Steel Institute (IISI); Yearbook of stainless steel applications, 2006.

[8] Helzel M. and Taylor I., “Pedestrian bridges in stainless steel”; *Building Series*, Volume 7, Brussels: Euro Inox, 2004.

[9] ArcelorMittal Building and Construction Support. Stainless steel in construction. Paris; 2009.

[10] ArcelorMittal Stainless Europe. Stainless steel for swimming pools. Paris; 2009.

[11] Saliba N. and Gardner L., “Experimental study of the shear response of lean duplex stainless steel girders”, *Engineering Structures*, Volume 46,pages 375-391, 2013.

[12] Olsson A., “Stainless steel plasticity-material modelling and structural applications”, PhD thesis, Lulea University of Technology, Sweden, 2001.

[13] Bleich H., "Buckling Strength of Metal Structures", McGraw-Hill Book Co. Inc, New York, N.Y., 1952.
[14] Timoshenko S. P. and Gere J. M., "Theory of Elastic Stability", McGraw-Hill Book Co. Inc, New York, N.Y., 1961.
[15] Basler K., Yen B. T., Mueller J. A. and Thürlimann B., "Web buckling tests on welded plate girders", Bulletin no 64, 1960.
[16] Porter D. M., Rockey K. C. and Evans H. R., "The collapse behaviour of plate girders loaded in shear", *Structural Engineer*, Volume 53(8), pages 313-325, 1975.
[17] Höglund T., "Design of thin plate I girders in shear and bending with special reference to web buckling." Bulletin no. 94. Royal Institute of Technology, Stockholm, Sweden; 1973.
[18] European Committee for Standardization (CEN), "Eurocode 3: design of steel structures - part 1-5: General rules – Plated structural elements." Brussel Cen, 1/5/2005, Brussel, 2005.
[19] Carvalho E. C. G., Van den Berg G. J. and Van der Merwe P., "Local shear buckling in cold-formed stainless steel beam webs." *Proceedings of the annual technical session*, Structural Stability Research Council, 1990.
[20] Shanmugam N. E. and Baskar K., "Steel–Concrete Composite Plate Girders Subject to Shear Loading", *Journal of Structural Engineering*, Volume129(9), pages 1230-1242, 2003.
[21] Aziz E. M., Kodur V. K., Glassman J. D., and Moreyra Garlock M. E., "Behavior of steel bridge girders under fire conditions", *Journal of Constructional Steel Research*, Volume 106, pages 11-22, 2015.
[22] Reis A., Lopes N. and Real P. V., "Numerical study of steel plate girders under shear loading at elevated temperatures", *Journal of Constructional Steel Research*, Volume 117, pages 1-12, 2016.
[23] Reis A., Lopes N. and Real P. V., "Shear–bending interaction in steel plate girders subjected to elevated temperatures", *Thin-Walled Structures*, Volume 104, pages 34-43, 2016.
[24] Girão Coelho A. M., Bijlaard F. S. K. and Kolstein H., "Experimental behaviour of high-strength steel web shear panels", *Engineering Structures*, Volume 31(7), pages 1543-1555, 2009.
[25] Yuan H.X., Wang Y.Q., Shi Y.J. and Gardner L., "Stub column tests on stainless steel built-up sections", *Thin-Walled Structures*, Volume 83, pages 103-114, 2014.
[26] Afshan S. and Gardner L., "The continuous strength method for structural stainless steel design", *Thin-Walled Structures*, Volume 68, pages 42-49, 2013.
[27] Ashraf M., Gardner L. and Nethercot D.A., "Compression strength of stainless steel cross-sections", *Journal of Constructional Steel Research*, Volume 62, pages 105-115, 2006.
[28] Young B. and Liu Y., "Experimental investigation of cold-formed stainless steel columns", *Journal of Structural Engineering*, Volume 129 No.2, pages 169-176, 2003.
[29] Zhao O., Rossi B., Gardner L. and Young B., "Stainless steel cross-sections under combined loading", Proceedings of Eurosteel, Naples Italy, pages 97-98, 2014.
[30] Cashell K.A. and Baddoo N.R., "Ferritic stainless steels in structural applications", *Thin-Walled Structures*, Volume 83, pages 169-181, 2014.
[31] Baddoo N. R., "Advances in structural stainless steel research", *Thin-Walled Structures*, Volume 83, page 1, 2014.
[32] Huang Y. and Young B., "Material properties of cold-formed lean duplex Stainless Steel Sections", *Thin-walled Structures*, Volume 54, pages 72-81, 2012.
[33] Huang Y. and Young B., "Stress–strain relationship of cold-formed lean duplex stainless steel at elevated temperatures", *Journal of Constructional Steel Research*, Volume 92, pages 103-113, 2014.
[34] Theofanous M. and Gardner L., "Testing and numerical modelling of lean duplex stainless steel hollow section columns", *Engineering Structures*, Volume 31, pages 3047-3058, 2009.
[35] Huang Y. and Young B., "Design of Cold-Formed Lean Duplex Stainless Steel Members in Combined Compression and Bending", *Journal of Structural Engineering*, Volume 141(5), pages 04014138, 2014.

[36] Sabila N. and Gardner L., "Cross-section stability of lean duplex stainless steel welded I-sections", *Journal of Constructional Steel Research*, Volume 80, pages 1-14, 2012.
[37] Huang, Y. and Young, B., "Experimental and numerical investigation of cold-formed lean duplex stainless steel flexural members", *Thin-walled Structures*, Vol. 73, pages 216-228, 2013.
[38] Theofanous M. and Gardner L., "Experimental and numerical studies of lean duplex stainless steel beams", *Journal of Constructional Steel Research*, Volume 66, pages 816-825, 2010.
[39] Westin E. M., "Microstructure and properties of welds in the lean duplex stainless steel LDX 2101®", Doctoral thesis Royal Institute of Technology Stockholm, 2010.
[40] Sorrentino S., Fersini M. and Zilli G., "Comparison between SAW and laser welding processes applied to duplex structures for bridges", *Welding International*, Volume 23(9), pages 687 698, 2009.
[41] Yuan H.X., Wang Y.Q., Shi Y.J. and Gardner L., "Residual stress distributions in welded stainless steel sections", *Thin-Walled Structures*, Volume 79, pages 38-51, 2014.
[42] Gardner L. and Cruise R.B., "Modelling of residual stresses in structural stainless steel sections", *Journal of Structural Engineering*, Volume 135(1), pages 42-53, 2009.
[43] Saliba N., Real E. and Gardner L., "Shear design recommendations for stainless steel plate girders", *Engineering Structures*, Volume 59, pages 220-228, 2014.
[44] Real E., Mirambell E. and Estrada I., "Shear response of stainless steel plate girders", *Engineering structures* , Volume 29(7), pages 1626-1640, 2007.
[45] Estrada I., Real E. and Mirambell E., "General behaviour and effect of rigid and nonrigid end post in stainless steel plate girders loaded in shear. Part I:experimental study", *Journal of Constructional Steel Research*, Volume 63(7), pages 970–984, 2007.
[46] Hassanein M.F., "Finite element investigation of shear failure of lean duplex stainless steel plate girders", *Thin-Walled Structures* , Volume 49(8),pages 964-973, 2011.
[47] Estrada I., Real E. and Mirambell E., "General behaviour and effect of rigid and nonrigid end post in stainless steel plate girders loaded in shear. Part II: extended numerical study and design proposal", *Journal of Constructional Steel Research*, Volume 63(7), pages 985-996, 2007.
[48] Sutton M., Wolters W., Peters W., Ranson W. and McNeill S., "Determination of displacements using an improved digital correlation method", *Image and Vision Comput*ing, Volume 1(3), pages 133-139, Aug. 1983.
[49] Luo P. F., Chao Y. J., Sutton M. A. and Peters W. H., "Accurate measurement of three-dimensional deformations in deformable and rigid bodies using computer vision", *Experimental Mechanics*, vol. 33, no. 2, pages 123-132, 1993.
[50] Sutton M. A., Orteu J.-J. and Schreier H. W., "Image Correlation for Shape, Motion and Deformation Measurements: Basic Concepts, Theory and Applications.", Springer US, 2009.
[51] Küntz M., Jolin M., Bastien J., Perez F. and Hild F., "Digital image correlation analysis of crack behavior in a reinforced concrete beam during a load test", *Canadian Journal of Civil Eng*ineering, Volume 33, no. 11, pages 1418-1425, 2006.
[52] Yoneyama S., Kitagawa A., Iwata S., Tani K. and Kikuta H., "Bridge deflection measurement using digital image correlation", *Experimental Techniques*, Vol(31)1, pages 34–40, 2007.
[53] Malesa M., Szczepanek D., Kujawínska M., Swiercz A. and Kołakowski P., "Monitoring of civil engineering structures using digital image correlation technique", *EPJ Web of Conferences*, volume 6, page 31014, 2010.
[54] Koltsida I. S., Tomor A. K. and Booth C. A., "The use of digital image correlation technique for monitoring masonry arch bridges", *7th International Conference on Arch Bridges*, pages 681-690, 2013.
[55] Santini-Bell E., Brogan P., Lefebvre P., Peddle J., Brenner B. and Sanayei M., "Digital Imaging for Bridge Deflection Measurement of a Steel Girder Composite Bridge", *TRB 90th Annual Meeting Compendium of Papers*, pages 1633, 2011.

[56] Tung S.-H., Shih M.-H. and Sung W.-P., "Applying the digital-image-correlation technique to measure the deformation of an old building's column retrofitted with steel plate in an in situ pushover test", *Sadhana,*Volume 39(3), pages 699–711, 2014.
[57] Kujawinska M., Malesa M., Malowany K., Piekarczuk A., Tyminska-Widmer L. and Targowski P., "Digital image correlation method: a versatile tool for engineering and art structures investigations", *Congress of the International Commission for Optics: Light for the Development of the World*, Volume 8011, pages R1–R8. SPIE, 2011.
[58] De Roover C., Vantomme J., Wastiels J. and Taerwe L., "Deformation analysis of a modular connection system by digital image correlation", *Experimenatal Techniques*, Volume 26(6), pages 37–40, 2002.
[59] Featherston C.A., Eaton M.J. and Holford K.M., "Imperfection sensitivity in plates - An assessment using DIC", *SEM XI International congress on experimental and applied mechanics*, 2008.
[60] Braga D. F. O., Ramos T., Eslami S., Tavares P. J., Infante V., de CastroP. M. S. T. and Moreira P. M. G. P., "Train passenger car floor panel testing using digital image correlation and strain gauges and comparison with finite element modelling", *Engineering Failure Analysis*, 2016.
[61] Ferreira M. D. C., Venturini W. S. and Hild F., "On the analysis of notched concrete beams: From measurement with digital image correlation to identification with boundary element method of a cohesive model", *Engineering Fracture Mechanics*, Volume 78(1), pages 71-84, 2011.
[62] Dutton M., Take W. A. and Hoult N. A., "Curvature Monitoring of Beams Using Digital Image Correlation", *Journal of Bridge Engineering*, Volume 19(3), page5013001, 2014.
[63] Souid A., Delaplace A., Ragueneau F. and Desmorat R., "Pseudodynamic testing and nonlinear substructuring of damaging structures under earthquake loading", *Engineering.Structures*, Volume 31(5),pages 1102-1110, 2009.
[64] Smith B. J., Kurama Y. C. and McGinnis M. J., "Design and Measured Behavior of a Hybrid Precast ConcreteWall Specimen for Seismic Regions", *Journal of Structural Engineering*, Volume 137(10), pages 1052–1062, 2011.
[65] De Wilder K., Lava P., Debruyne D., Wang Y., De Roeck G. and Vandewalle L., "Experimental investigation on the shear capacity of prestressed concrete beams using digital image correlation", *Engineering Structures*, Volume 82(1), pages 82-92, 2015.
[66] Ghafoori E. and Motavalli M., "Analytical calculation of stress intensity factor of cracked steel I-beams with experimental analysis and 3D digital image correlation measurements", *Engineering Fracture Mechanics*, Volume 78(18),pages 3226-3242, 2011.
[67] Hild F., Roux S., Guerrero N., Eugenia Marante M. and Flórez-López J., "Calibration of constitutive models of steel beams subject to local buckling by using digital image correlation", *European Journal of Mechanics A - Solids*, Volume 30(1), pages 1–10, 2011.
[68] Sozen S. and Guler M., "Determination of displacement distributions in bolted steel tension elements using digital image techniques", *Optics and Lasers in Engineering*, Volume 49(12), pages 1428-1435, 2011.
[69] Shih M.-H. and Sung W.-P., "Developing Dynamic Digital Image Correlation Technique to Monitor Structural Damage of Old Buildings under External Excitation", *Shock and Vibration*, 2014.
[70] Tran A. T., Veljkovic M., Rebelo C. and da Silva L. S., "Buckling Observation of Door Openings for Wind Turbine Towers", *Nordic Steel Construction Conference 2015*. 25-Sep-2015.
[71] Orteu J.-J., "3-D computer vision in experimental mechanics", *Optics and Lasers in Engineering*, Volume 47(3-4), pages 282-291, 2009.
[72] www.matchidmbc.be
[73] European Committee for Standardization (CEN), "EN ISO 6892 Metallic materials – Tensile testing –Part 1: Method of test at room temperature" Brussel Cen, 2009.
[74] European Committee for Standardization (CEN), "EN 1090-2 Execution of steel structures and aluminium structures – Part 2: Technical requirements for steel structures" Brussel Cen, 2009.
[75] Rossi B. and Li Y., " Extension of the DSM to welded H profile cross-sections." *Proceedings of Structural Engineering, Mechanics and Computation*, 2013.